ELSEVIER

Thermochimica Acta 330 (1999) 3–19

thermochimica acta

The practical applicability of TMDSC to polymeric systems

Rolf Scherrenberg*, Vincent Mathot, Annick Van Hemelrijck

DSM Research, PO Box 18, NL-6160MD, Geleen, Netherlands

Received 2 October 1998; accepted 11 January 1999

Abstract

The practical applicability and the relevance of a classification of processes into three different regimes is examined based on some typical TMDSC experiments. It is demonstrated that this classification, simply based on the presence and temperature susceptibility of an excess process, is very useful to identify and understand phenomena observed with TMDSC.

The ability to separate the base-line heat capacity from excess phenomena is undoubtedly the most valuable feature of TMDSC. Nonetheless, one has to realize that this feature is restricted to excess processes that are not susceptible to the temperature modulation such as for instance curing and enthalpy recovery. Crystallization and melting processes, on the other hand, are susceptible to the temperature modulation and thus the complex heat capacity is in that case not uniquely determined by the base-line heat capacity. In addition, the strong temperature dependence of the kinetics in combination with the generally large heat flow, imply that the conditions applied are very critical to obtain a reliable complex heat capacity. In spite of these serious limitations it is demonstrated that TMDSC can provide additional insight in the crystallization and melting behaviour using (step-wise) quasi-isothermal measurements (i.e. β_0=0).

Keywords: DSC; TMDSC; Polymers; Glass-transition; Curing; Crystallization; Melting; Excess heat capacity; Base-line heat capacity; Regime; Quasi-isothermal

1. Introduction

Since the introduction of temperature modulated differential scanning calorimetry (TMDSC) in 1993, an impressive number of papers have appeared describing its potential applicability in a wide variety of fields such as absolute heat capacity determination [1,2], thermal conductivity [3,4], glass transition region [5–16], curing [17–23], miscibility [24–27] as well as crystallization and melting [28–40]. From this viewpoint, TMDSC can undoubtedly be regarded as a valuable extension of conventional DSC, that is in particular advantageous in the case of overlapping processes. Unfortunately, its applicability is generally not very straightforward and dependent on a number of important aspects such as [41]:

1. Material invariance on the time-scale of modulation
2. Linearity of the process (input $ax_1+bx_2 \rightarrow$ output ay_1+ay_2)
3. The time-scale of a process and its susceptibility to the temperature modulation
4. Instrument performance (linearity, steady state)

Moreover, the experimental conditions and data evaluation are, apart from its limited frequency range, more critical as compared to other dynamical techni-

*Corresponding author. E-mail: rolf.scherrenberg@dsm-group.com

0040-6031/99/$ – see front matter
PII: S0040-6031(99)00036-2

ques such as dynamical mechanical thermal analysis (DMTA) and dielectric thermal analysis (DETA). In TMDSC the temperature plays not only a role in the dynamic input but is also used in the underlying linear temperature variation and the corresponding heat flow response. In that respect, a mechanical equivalent of a TMDSC experiment with an underlying scanning rate β_0 would be a DMTA measurement on top of a stress–strain measurement.

The above respects have been outlined in more detail in a recent paper [41]. Based on a theoretical description of the heat flow response using the full heat capacity concept, it was demonstrated that processes studied with TMDSC can be classified into three distinct regimes, depending on the time-scale and the susceptibility of the process to the temperature modulation. In this paper, the relevance of these different regimes will be validated on the basis of some typical TMDSC experiments. Furthermore, the applicability of TMDSC in the melting and crystallization region will be discussed in more detail.

2. Experimental

The (TM)DSC experiments were carried out with three different DSC instruments, namely Perkin-Elmer Pyris-1, TA Instruments DSC 2920 and Mettler DSC-821. The instrument used for a particular experiment will be denoted in the caption of the corresponding figure. The TA Instruments heat flux DSC 2920 was equipped with a refrigerated cooling system. Helium was used as purge gas (25 ml/min). The temperature was calibrated using cyclohexane and indium. The latter was also used for enthalpy calibration. The heat capacity was calibrated with a linear polyethylene material NIST SRM1475 [42] at 150°C ($c_{p_b} = 2.57\,\mathrm{J/(g^\circ C)}$ [43]). For the calibrations, the same pan type and period of modulation were used as in the corresponding experiments. For each experiment, a modulation period of 60 s was applied. Perforated aluminium pans (50 μl Perkin-Elmer) were used.

The Perkin-Elmer Pyris-1 power-compensating DSC was equipped with a Cryofil^{TM} cooling system operating at liquid nitrogen temperature. A 90/10 mixture of neon/helium was used as purge gas (25 ml/min). The temperature was calibrated using adamantane, indium and lead. Indium was also used for energy calibration. An empty pan measurement (50 μl perforated aluminium Perkin-Elmer pan) was subtracted for all measurements.

Conventional heat capacity experiments were performed on a Mettler DSC-821 heat flux DSC equipped with a refrigerated cooling system. Nitrogen was used as purge gas (80 ml/min). The temperature and energy was calibrated with indium, lead and zinc using a standard procedure in the Mettler software. The absolute heat capacity was determined according to DIN 51007 using a sapphire and an empty pan measurement. Perforated aluminium 40 μl Mettler pans were used.

3. Results and discussion

3.1. The base-line heat flow Φ_b (regime I)

Regime I is representative for the thermal behaviour of materials in the absence of any excess heat flow response (i.e. Φ_e=0) such as enthalpy recovery, chemical reactions (e.g. curing) and crystallization and melting. A typical example of regime I is the thermal behaviour of an amorphous polymer around the glass-transition region during cooling (i.e. absence of enthalpy recovery) as in illustrated in Fig. 1 for an amorphous styrene–maleic acid (SMA) copolymer.

The heat flow response in regime I is uniquely determined by the base-line heat capacity c_{p_b} of the material studied which is connected with the torsional vibrations and segmental motions. In the glassy state, relaxation processes are related to kinetically simple, quasi-independent motional events with relaxation times in the order of 10^{-13} s. These motional events are commonly denoted as non-cooperative motions, although several atoms participate.

The glass transition region, on the other hand, corresponds with motions of molecular segments. The relaxations times $\tau(T)$ corresponding to these so called cooperative motions are considerably larger as compared with the non-cooperative motions and can be, depending on the temperature, on the time-scale of TMDSC (10–100 s) or even larger.

The time-scales of the cooperative and non-cooperative motions are represented schematically in Fig. 2 by time distributions of the heat flow response.

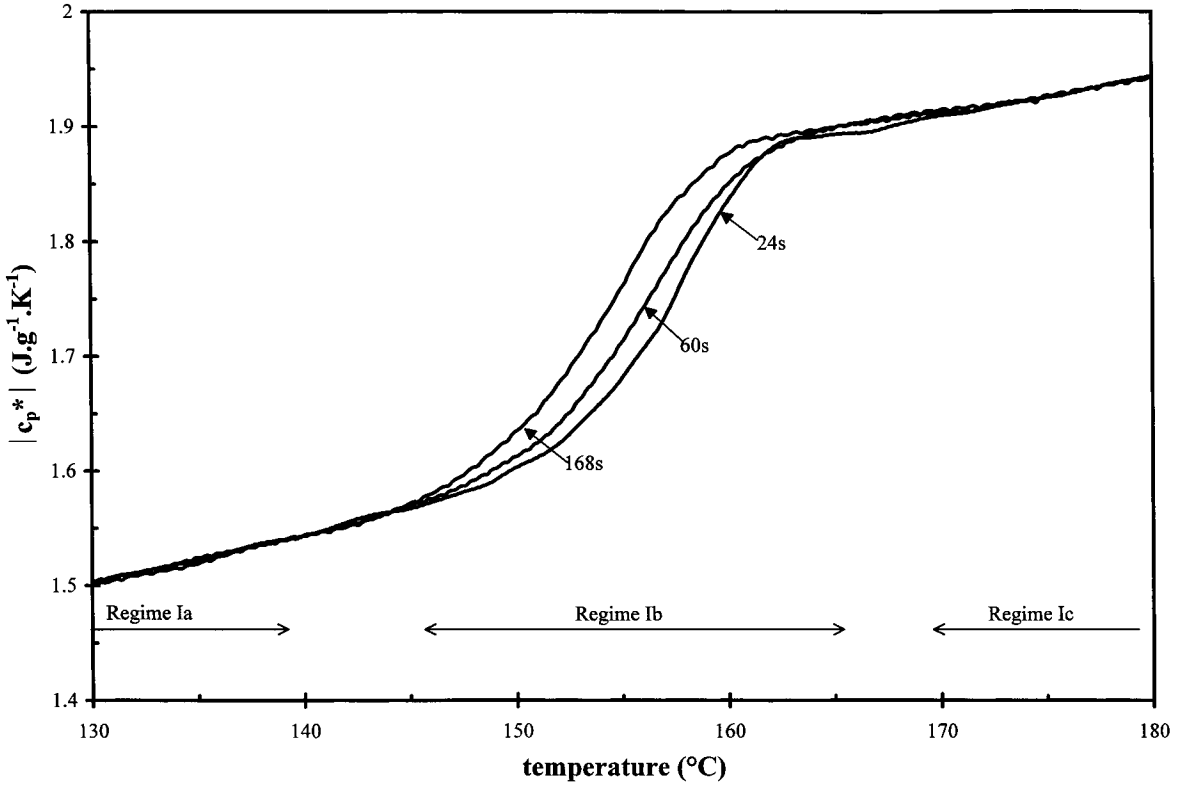

Fig. 1. The magnitude of the complex heat capacity $|c_p^*|$ versus the temperature for styrene–maleic acid (SMA) in the glass-transition region during cooling. A saw-tooth-modulation was applied with (a) p=168 s; A_T=2.1°C; β_0=1°C/min; (b) p=60 s; A_T=1°C; β_0=2°C/min; (c) p=24 s; A_T=0.5°C; β_0=3°C/min (Perkin-Elmer Pyris-1).

For illustrative purposes, these time distributions are represented by a Gaussian distribution. Although such a distribution is most probably not a correct representation of the time-scales involved, its exact shape is not critical for the concept described. The time-scales related to the temperature modulation (i.e. $p=2\pi/\omega_0$) and β_0 are also illustrated in Fig. 2. The time-scale corresponding to β_0 has been positioned to the right of that of the temperature modulation because in view of the requirement of material invariance, the temperature variation due to the underlying scanning rate β_0 has to be in principle smaller than the temperature amplitude A_T and preferably zero within a modulation period (i.e. $\beta_0/(A_T\omega_0)<1$. In practice, however, this precondition in regime I is not as critical as for instance during crystallization and melting (regime III). This is related to the fact that the temperature dependence of the base-line heat capacity is substantially smaller in comparison with the temperature dependence of the excess heat flow connected with crystallization and melting. The position of β_0 on the time-scale (Fig. 2) has been chosen somewhat arbitrary and can shift to a certain extent with the temperature, depending on the activation energy of the process studied. As illustrated in Fig. 2, the distribution corresponding to the non-cooperative motions is always situated completely left of the time-scale probed with (TM)DSC (10–100 s) because the time-scale of this type of motions is considerably shorter. The heat flow corresponding to these motions can therefore be regarded as time independent (i.e. instantaneous response). On the other hand, the time-scale of the cooperative motions can, due to the time–temperature interrelationship, be in the order of the time-scales probed with (TM)DSC and hence can overlap at certain temperatures with the time-scale of modulation. Accordingly, three subregimes can be identified (Figs. 1 and 2).

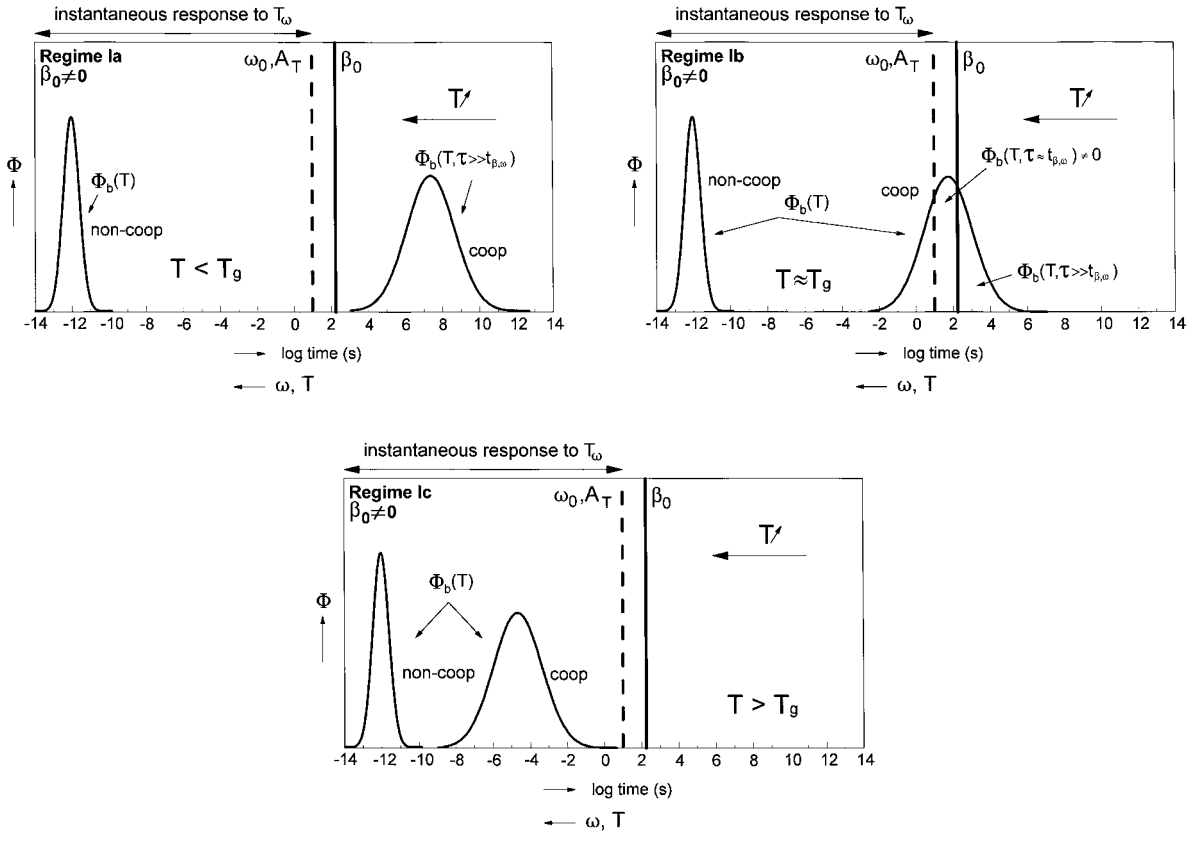

Fig. 2. Schematic representation of regime I. (a) and (c) are representative for a material below and above the glass-transition region, respectively. (b) is illustrative for the glass-transition region.

In regime Ia (Fig. 2(a)), the time-scale of the heat flow response Φ_e corresponding to the cooperative motions are located completely right of the modulation window, signifying that, in contrast to the non-cooperative motions, the cooperative motions are slow in comparison with the time-scale of the experiment and will therefore not contribute to the heat flow response Φ_b. This regime is useful to describe the thermal properties of an amorphous polymer below the glass transition region (Fig. 1).

In regime Ic (Fig. 2(c)), the time-scales of the heat flow response corresponding to both the cooperative and non-cooperative motions are situated completely left of the modulation window. Hence, the heat flow response, comprising both type of motions, will follow the applied temperature program instantaneously and can be regarded as time independent of the time-scale of the modulation (Fig. 1).

The time-independence of the heat flow response in regime Ia and Ic implies that the phase shift is by definition zero. Therefore, the use of the full deconvolution method (i.e. separation into an in- and out-of-phase heat capacity) in these regimes has no relevance. For the same reason, the base-line heat capacity based on both the underlying and modulated temperature variation has to be identical in these regimes, as is illustrated in Fig. 1. This also implies that any deviation of the phase angle δ from zero in regime Ia and Ic has to be related to artefacts originating from the sample (e.g. thermal transfer) and/or instrument.

The above arguments no longer hold in the glass-transition region (regime Ib). In the glass-transition region, the time-scale of the heat flow response corresponding to the cooperative motions overlaps with the time-scale of the temperature modulation (Fig. 2(b)); i.e. the heat flow response comprises a

time-dependent contribution and therefore the phase angle is no longer zero. In this case, the use of the full deconvolution method is in principle relevant, although in practice the phase angles are generally so small that in most cases the use of the simple deconvolution (i.e. phase information neglected (δ=0)) can still be justified.

The dependence of the glass-transition temperature on the time-scale of the experiment, as schematically represented in Fig. 2, is also found experimentally for a styrenic–maleic acid (SMA) copolymer (Fig. 1). The glass-transition region shifts towards higher temperatures on increasing the temperature modulation ω_0 which is in good agreement with earlier studies on polystyrene [14,15]. This phenomenon can simply be explained by the fact that the relaxation time distribution corresponding to the cooperative motions will overlap with the time-scale of modulation at relatively higher temperatures on increasing ω_0.

3.2. The heat flow in the presence of excess phenomena (regimes II and III)

Additional to the heat flow response Φ_b connected with the baseline heat capacity, excess phenomena such as enthalpy recovery, crystallization and melting, and chemical reactions can contribute to the total heat flow response. The evaluation of the (TM)DSC heat flow response in the presence of such excess phenomena is less straightforward in comparison with regime I because the magnitude as well as the temperature dependence of the excess heat flow response Φ_e are generally considerably larger than that of Φ_b.

In case of an excess process, both the variation of the mass fraction w_i with temperature ($\partial w_i/\partial T$) and time ($\partial w_i/\partial t$) are of importance. Firstly, the time-scale (i.e. kinetics) of the excess process ($\partial w_i/\partial t$) has in all cases to be significantly longer than the time-scale of

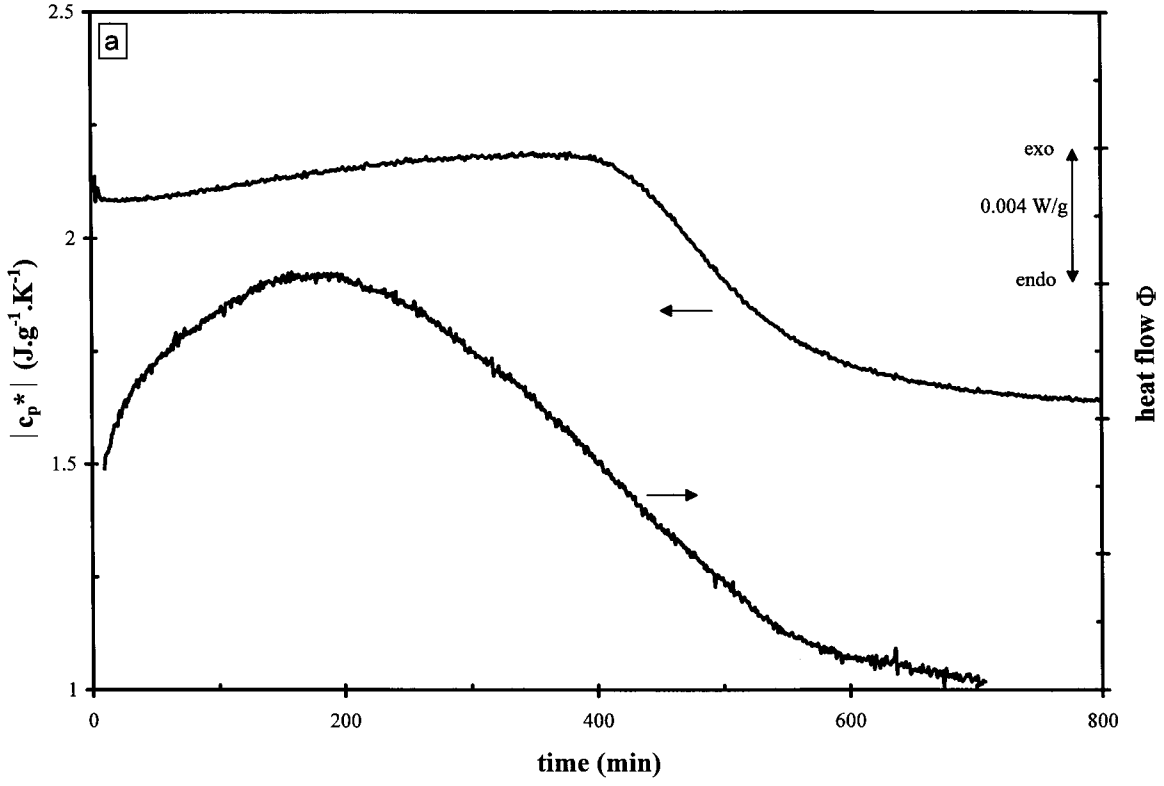

Fig. 3. (a) Quasi-isothermal curing of an epoxy-amine thermosetting system at 40°C. A sinusoidal modulation was applied with A_T=0.5°C and p=60 s (TA Instruments); (b) residual cure after the quasi-isothermal curing. The experimental conditions applied were A_T=0.3°C, p=60 s and an underlying heating rate β_0 of 2.5°C/min.

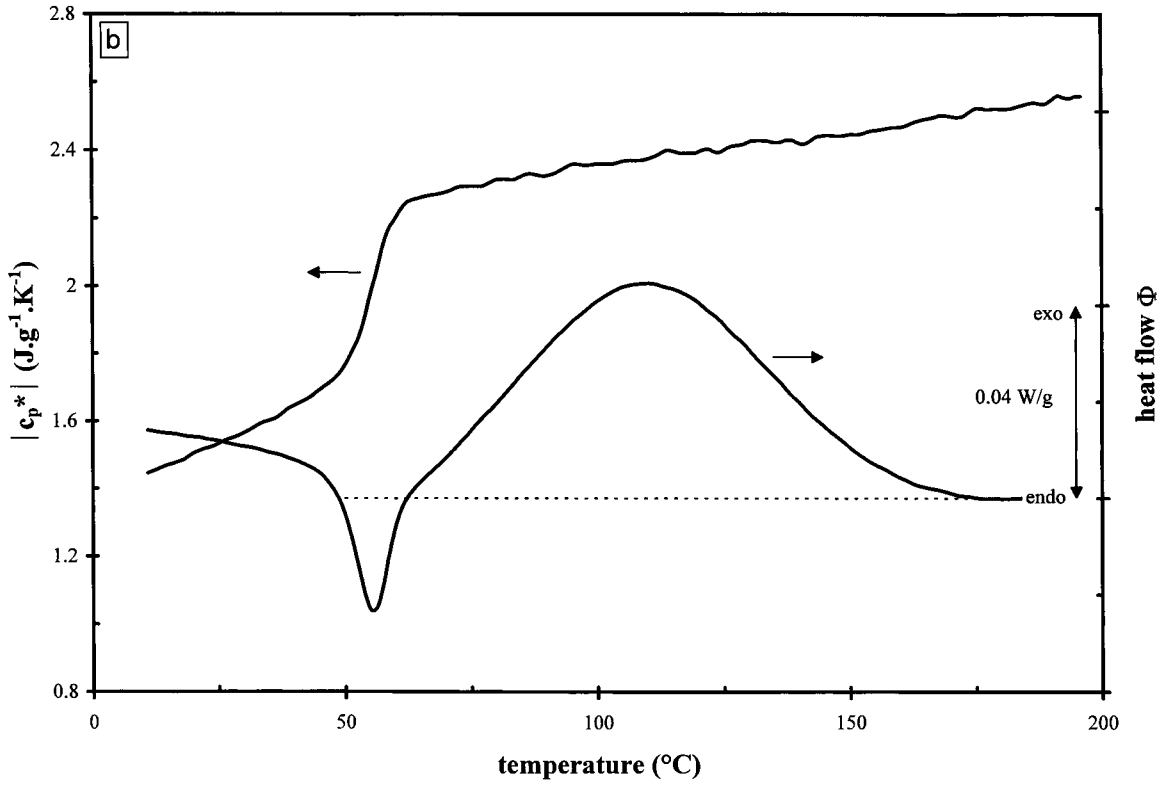

Fig. 3. (*Continued*)

modulation because otherwise the material properties vary during a modulation period and thus the requirement of material invariance is violated. For the same reason, the variation of the mass fraction w_i during a modulation as a result of the underlying scanning rate β_0 has to be negligible, $\partial w_i/\partial T_\beta=0$, implying that quasi-isothermal conditions (i.e. $\beta_0=0$) are preferable. Moreover, the susceptibility of the mass fraction w_i to the temperature modulation T_ω is of significance. In this respect, two different regimes, namely regimes II and III, can be distinguished.

In regime II, the existing mass fraction w_i is not influenced by the temperature modulation (i.e. $\partial w_i/\partial T_\omega=0$). In other words, there is no contribution of the excess process to the modulated heat flow response Φ_ω as a result of the temperature modulation (i.e. $c_{p_e}=0$).

In regime III, on the other hand, the existing mass fraction w_i is varied by the temperature modulation (i.e. $\partial w_i/\partial T_\omega\neq 0$).

3.2.1. Regime II ($\partial w_i/\partial T_\omega=0$)

A very important feature of regime II is that, due to the insensitivity of the excess process to the temperature modulation (i.e. $\partial w_i/\partial T_\omega=0$), the modulated heat flow response Φ_ω is uniquely determined by the base-line heat capacity c_{p_b}. This enables the separation between the base-line heat capacity and an excess heat flow contribution which proves to be very useful in the case of overlapping processes involving excess processes such as enthalpy recovery, cold crystallization and heat of reaction superimposed on a vitrification process.

A typical example of regime II is the curing of a resin [17–23], as is illustrated in Fig. 3 for an epoxy-amine thermosetting system. The heat flow curve in Fig. 3(a) represents the heat flow Φ generated by the quasi-isothermal curing and is in principle similar to that obtained with conventional isothermal DSC experiments. The modulated heat flow response Φ_ω, on the other hand, comprises no contribution from the

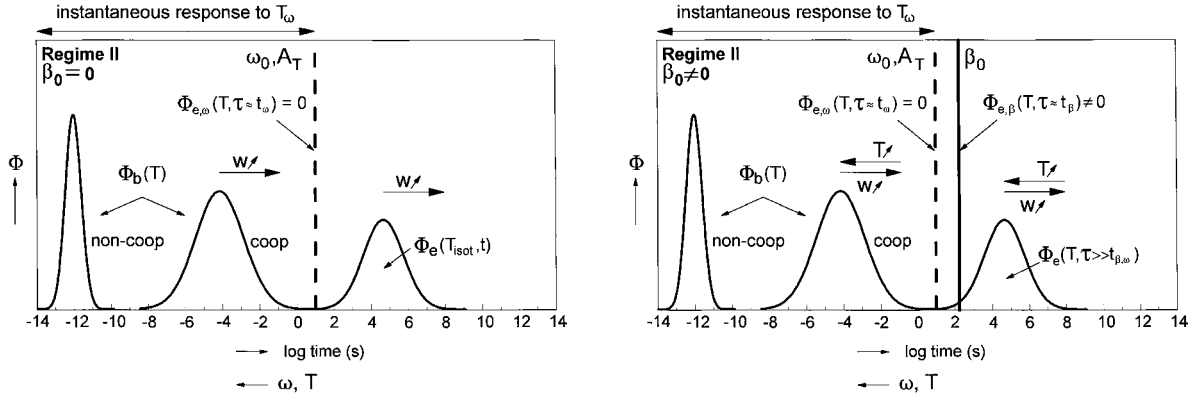

Fig. 4. Schematic representation of regime II. (a) and (b) are illustrative for a curing process under quasi-thermal (β_0=0) conditions and with an underlying linear temperature variation T_β ($\beta_0 \neq 0$), respectively.

excess process because the process is not susceptible to the temperature modulation. Consequently, the observed gradual decrease of the magnitude of the complex heat capacity $|c_p^*|$ in Fig. 3(a) is uniquely determined by the decrease of the base-line heat capacity during vitrification process.

The quasi-isothermal curing process is illustrated schematically in Fig. 4(a) by a shift of the relaxation time distribution towards longer time-scales on increasing conversion w_i, as a result of the corresponding reducing molecular mobility. At a certain point, the relaxation time distribution representing the cooperative motions shifts through the time-scale of the temperature modulation which is accompanied by a decrease of the base-line heat capacity (i.e. vitrification). The modulated heat flow response comprises a time-dependent contribution as the time-scales of the relaxation process and the temperature modulation overlap and consequently the phase angle δ is no longer zero (cf. regime Ib). For this reason, the phase angle δ gives additional information about the vitrification process, as already found experimentally by van Assche et al. [22,23].

A TMDSC experiment with an underlying heating rate β_0 after the quasi-isothermal curing (Fig. 3(a)) is depicted in Fig. 3(b). In analogy with the quasi-isothermal experiments, the variation of the base-line heat capacity can be separated from the excess heat flow Φ_e connected with the residual cure due to the insensitivity of the curing process to the temperature modulation. The heat flow curve in Fig. 3(b) also exhibits a large enthalpy recovery effect which is frequently observed after isothermal curing. This excess process is also insensitive to the temperature modulation and therefore does not contribute to the variation of the complex heat capacity in the glass-transition region. The ability of TMDSC to separate enthalpy recovery effects from the variation of the base-line heat capacity in the glass-transition region is a real added value as compared with conventional DSC in studying the glass-transition region of polymeric materials in general.

A schematic representation of regime II with an underlying scanning rate β_0 is shown in Fig. 4(b). The position of the relaxation time distributions is much more arbitrary as compared with Fig. 4(a) because of the complex and generally counteracting influence of the temperature and the degree of conversion on the molecular mobility. Increasing the temperature increases the molecular mobility but also increases the conversion rate ($\partial w_i/\partial t$) of the curing process. The latter, on the other hand, will result in a lower molecular mobility. For these reasons, the time-scales corresponding to Φ_b and Φ_e as illustrated in Fig. 4(b), are chosen arbitrarily and can be very dependent on the temperature and process studied.

3.2.2. Regime III ($\partial w_i/\partial T_\omega \neq 0$)

In contrast to regime II, the excess process is influenced by the temperature modulation in regime III (i.e. $\partial w_i/\partial T_\omega \neq 0$). An illustrative example of such an excess process in the quasi-isothermal crystallization of a linear polyethylene NIST SRM1484 [42] (Fig. 5). The heat flow curve in Fig. 5 is representative

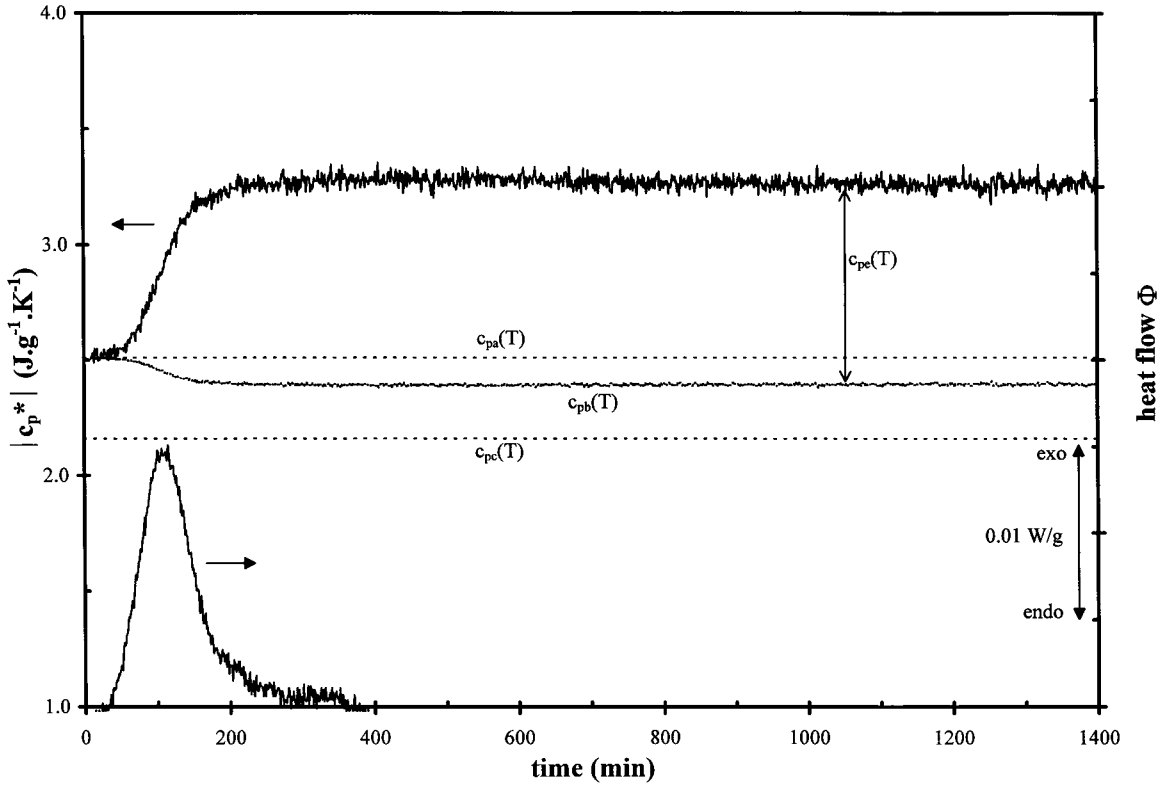

Fig. 5. Quasi-isothermal crystallization of linear polyethylene (NIST SRM1484) at 128.5°C. A sinusoidal temperature modulation was applied with A_T=0.1°C and p=60 s (TA Instruments). The base-line heat capacity c_{p_b} has been calculated on the basis of the variation of degree crystallinity with time, based on the ratio between the integrated heat flow with time and the literature value for the heat of fusion of 100% crystalline polyethylene, and the literature values for the amorphous and crystalline heat capacity (c_{p_a} and c_{p_c}) and 128.5°C [43–45].

for the heat flow generated during the quasi-isothermal crystallization. From that viewpoint, the crystallization process at this quasi-isothermal temperature is apparently completed after about 300 min. The magnitude of the complex heat capacity $|c_p^*|$, on the other hand, shows a gradual increase with time and finally reaches a constant value which remains constant up to the end of the experiment (i.e. 1400 min). Toda et al. [32,33] have reported a similar increase of $|c_p^*|$ for a comparable linear polyethylene sample (NIST SRM 1483) [42]. Quasi-isothermal crystallization experiments have also been described for other polymers such as polyethylene terephthalate [38,39], PEEK [35], polypropylene [46] and polycaprolacton [47]. However, the absolute variation of $|c_p^*|$ during quasi-isothermal crystallization for these polymers is noticeably smaller in comparison with polyethylene and in the case of polycaprolacton [47] even a small decrease of $|c_p^*|$ is observed on crystallization. Simply based on the change of the base-line heat capacity c_{p_b} one should expect a decrease of the base-line heat capacity on crystallization because the heat capacity of the crystalline phase is smaller than that of the amorphous phase [43–45][1] as illustrated in Fig. 5 for the linear polyethylene studied (NIST SRM 1484). This implies that $|c_p^*|$ during the quasi-isothermal crystallization is not uniquely determined by the base-line heat capacity but also comprises an additional excess heat flow contribution $\Phi_{e,\omega}$ that instantaneously follows the temperature modulation (i.e. $\partial w_i/\partial T_\omega \neq 0$). In that respect, the difference between $|c_p^*|$ and the base-line

[1]WWW (Internet), URL: http://funnelweb.utcc.utk.edu/~athas. For a general description see also [45].

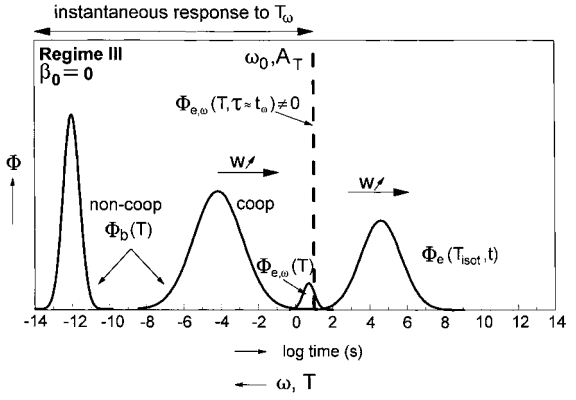

Fig. 6. Schematic representation of a quasi-isothermal crystallization (regime III).

heat capacity is representative for the so called excess heat capacity c_{p_e}. The time-independent heat flow contribution is represented schematically in Fig. 6 by an additional relaxation time distribution for $\Phi_{e,\omega}$ near the time-scale of modulation. A plausible explanation of the instantaneous excess heat flow contribution is, as already suggested by Wunderlich et al. [39,40], that a fraction of the crystalline material present at a specific time and temperature reversibly melts and crystallizes as a result of the temperature modulation. From that viewpoint, the variation of the excess heat capacity with time will most probably correlate with the fraction of crystallized material present (Fig. 7). The analogy between the variation of the excess heat capacity and the integrated heat flow with time at different quasi-isothermal temperatures (Fig. 7) seems to be in line with this view.

The above results show that TMDSC offers added value to study the melting and crystallization behaviour of polymeric materials. However, one has to realize that the experimental conditions for a meaningful TMDSC experiment in regime III are very critical and generally implying very long measurement times. Already in the most simple case, the quasi-isothermal crystallization, the isothermal crystallization temperature has to be chosen such that the variation of the degree of crystallinity (i.e. $\partial w_i/\partial t$) during a modulation period is negligible, otherwise the requirement of material invariance is violated. Secondly, the crystallization kinetics should not be influenced by the temperature amplitude applied. The latter precondition is not very obvious because of the commonly large temperature dependence of the crystallization kinetics. Fig. 8 shows a profound dependence of the crystallization kinetics on the temperature amplitude for linear polyethylene (NIST SRM 1484). Both $|c_p^*|$ and the heat flow curve shift towards smaller time-scales on increasing the temperature amplitude from 0.1°C to 1.6°C. This phenomenon is of course related to the larger temperature window ($T_0 \pm A_T$) on increasing the temperature amplitude A_T. The crystallization rate will be significantly slower for $T_0 - 0.1$°C as compared with $T_0 - 1.6$°C. The simultaneous increase of $|c_p^*|$ (Fig. 8) with the temperature amplitude applied can be explained along the same line, namely the larger the temperature window, the larger fraction of crystalline material that is susceptible to the temperature modulation.

The observed variation of the crystallization kinetics $\partial w_i/\partial t$ with the temperature amplitude applied combined with the intrinsic violation of material invariance (i.e. $\partial w_i/\partial T_\omega \neq 0$) imply that the use of the linear response theory and consequently the phase angle δ is disputable. Moreover, the amplitude of the first harmonic obtained from Fourier analysis contains only part of the information and therefore the complex heat capacity is more or less meaningless. The relevance of the complex heat capacity becomes even more questionable in case an underlying scanning rate β_0 is applied to study the whole melting and crystallization region. Apart from the question of material invariance and linearity, one also has to realize that the excess heat flow generated during melting and especially crystallization is generally large. In combination with the intrinsic poor heat conductivity, maintenance of steady state in the melting and crystallization region is not evident. The latter can be easily checked by a plot of the heat flow response versus the temperature for a certain period of time [10]. Such so called Lissajous representations (Fig. 9) for the linear polyethylene sample studies (NIST SRM 1484) show large distortions in the crystallization and melting region, indicating that the sample for this temperature program is far from steady state. Consequently, any evaluation of the modulated heat flow response in this temperature range, including the determination of $|c_p^*|$, is meaningless. This signifies the importance of checking maintenance of steady state prior to evaluation of the data.

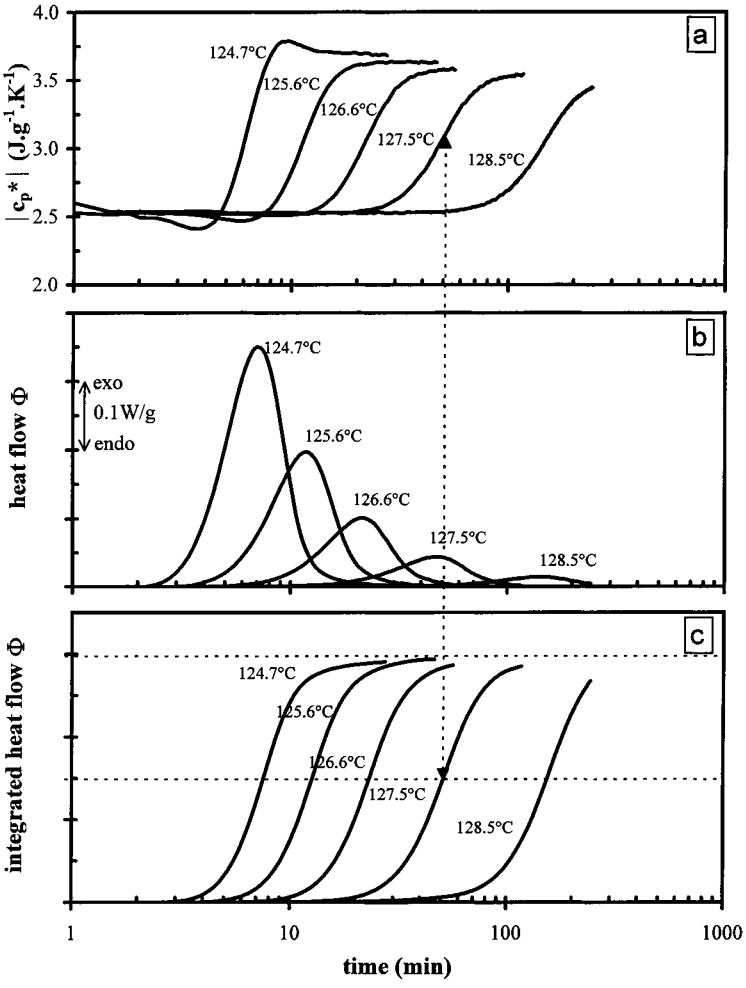

Fig. 7. Quasi-isothermal crystallization of linear polyethylene (NIST SRM1484) at different temperatures. A sinusoidal temperature modulation was applied with A_T=0.4°C and p=60 s (TA Instruments). (a) The magnitude of the compled heat capacity $|c_p^*|$ versus time; the initial deviation of $|c_p^*|$ at the lower quasi-isothermal temperatures is related to the fact that, due to the relatively fast crystallization, the first modulation cycles are not very reliable; (b) heat flow response Φ versus time; the apparent decrease of the heat flow response with the crystallization temperature is misleading and is caused by the logarithmic time-scale applied; (c) integrated heat flow response versus time.

As a result of the criticality of the temperature program used, so called step-wise quasi-isothermal temperature programs nowadays become more popular to study the melting and crystallization region. The magnitude of the complex heat capacity $|c_p^*|$ for the linear polyethylene studied (NIST SRM 1484) during both step-wise quasi-isothermal heating and cooling is depicted in Fig. 10. This figure shows a significant variation of $|c_p^*|$ during both melting and crystallization. Comparison of $|c_p^*|$ and the absolute heat capacity as measured with conventional DSC reveals that the variation of the heat capacity connected with temperature reversible melting and crystallization is in the order of a few percent (1–5%) of the total heat capacity variation during melting and crystallization (Fig. 11).

Analogous to the quasi-isothermal crystallization (Fig. 5), the magnitude of the complex heat capacity $|c_p^*|$ (Fig. 10(a)) initially increases around the crystallization temperature (±128°C). On further lowering of the temperature, $|c_p^*|$ decreases step-wise. This decrease is most probably related to an increasing

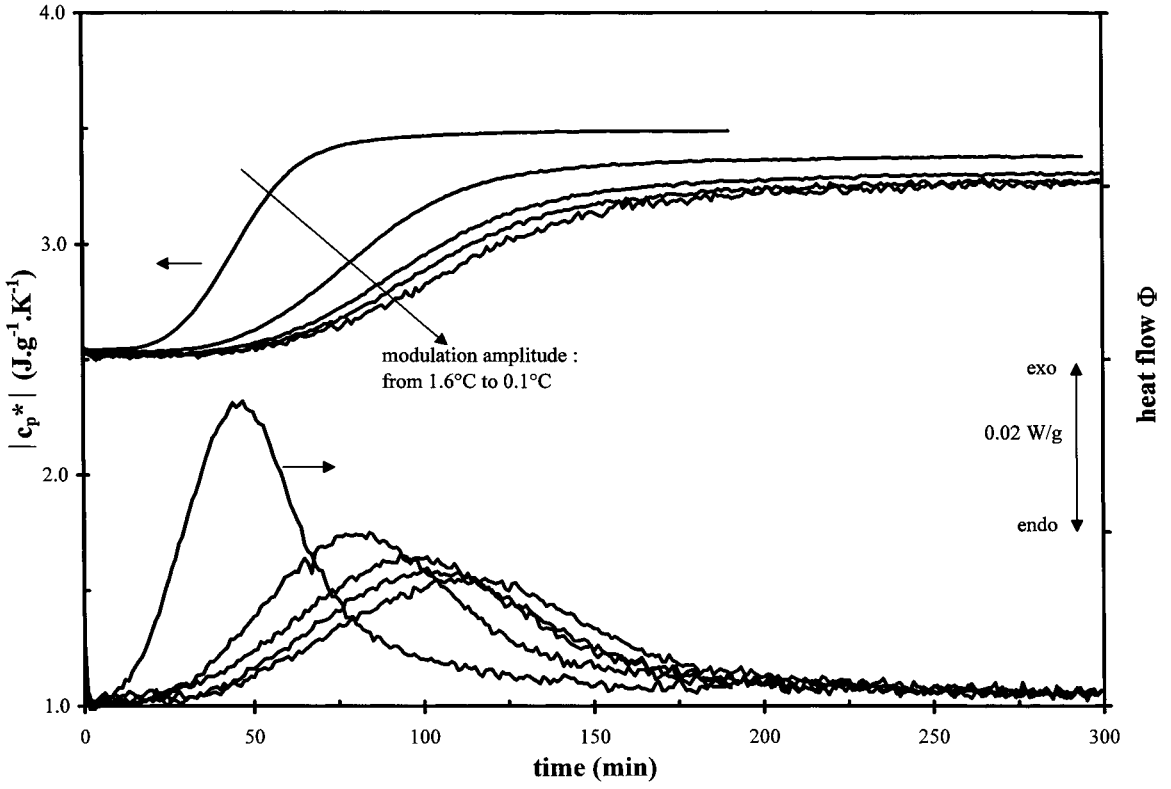

Fig. 8. The effect of the modulation amplitude ($0.1°C<A_T<1.6°C$) on the quasi-isothermal crystallization of linear polyethylene (NIST SRM1484) at 128.5°C. A sinusoidal temperature modulation was applied with p=60 s (TA Instruments).

fraction of crystalline material with a certain perfection and size that it is no longer susceptible to the temperature modulation on further lowering of the temperature. Noteworthy is that 30°C below the initial crystallization temperature of linear polyethylene there is still a detectable fraction of reversible melting and crystallization, as indicated by the fact that $|c_p^*|$ is still notably larger than the heat capacity corresponding to the amorphous phase. In analogy with crystallization, the increase of $|c_p^*|$ in the melting region (Fig. 10(b)) can be explained by an increasing susceptibility of the crystalline material to the temperature modulation on increasing the temperature. In contrast to step-wise quasi-isothermal cooling (Fig. 10(a)), however, the step-wise quasi-isothermal heating experiment (Fig. 10(b)) exhibits a significant decrease $|c_p^*|$ during the quasi-isothermal waiting time. At higher temperatures, the quasi-isothermal waiting time of 60 min is clearly insufficient to reach an equilibrium state. This phenomenon could be attributed to reorganization. Similar to annealing, the crystal size and perfection will be enhanced during the quasi-isothermal waiting time, resulting in a smaller fraction that is susceptible to the temperature modulation.

Above reasoning suggest that the variation of $|c_p^*|$ during the quasi-isothermal waiting time is very dependent on the thermal history. This is confirmed in Fig. 12(a) for a linear low density polyethylene (LLDPE). The double melting behaviour of this material, connected with the heterogeneous intra- and intermolecular distribution of the comonomer, is known to be very dependent on the thermal history [48]. A sample that previously has been cooled down with 20°C/min shows a considerable decrease of $|c_p^*|$ during the quasi-isothermal waiting time while the same sample after a step-wise quasi-isothermal cooling experiment with an average cooling rate of 0.033°C/min exhibits only a relatively small variation (Fig. 12(a)). Nevertheless, $|c_p^*|$ in the latter case is still

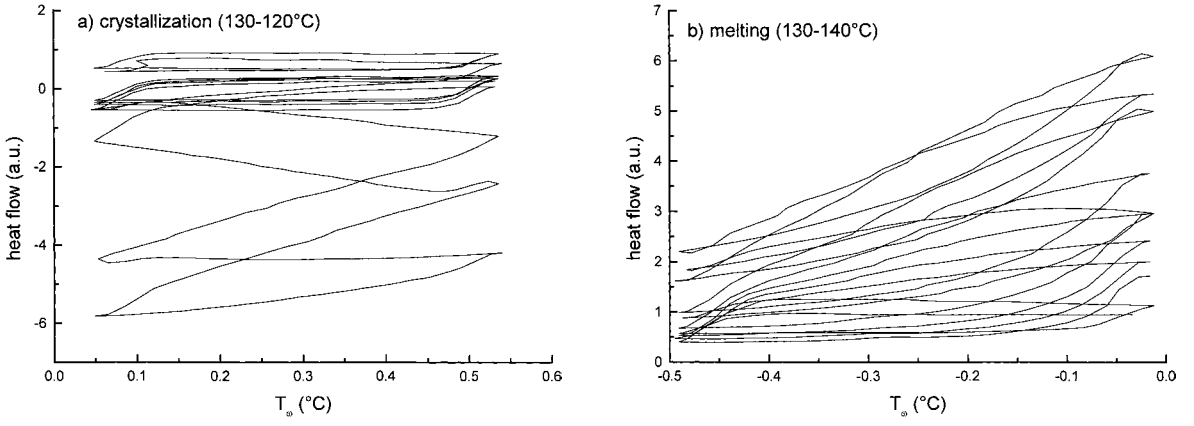

Fig. 9. Lissajous figures in the crystallization (a) and melting (b) region of linear polyethylene (NIST SRM1484). A so called iso-scan modulation was applied with a temperature step of 1°C (1°C/min) followed by an isothermal waiting time of 60 s. For the preparation of the Lissajous figure a linear temperature variation of 0.5°C/min has been subtracted.

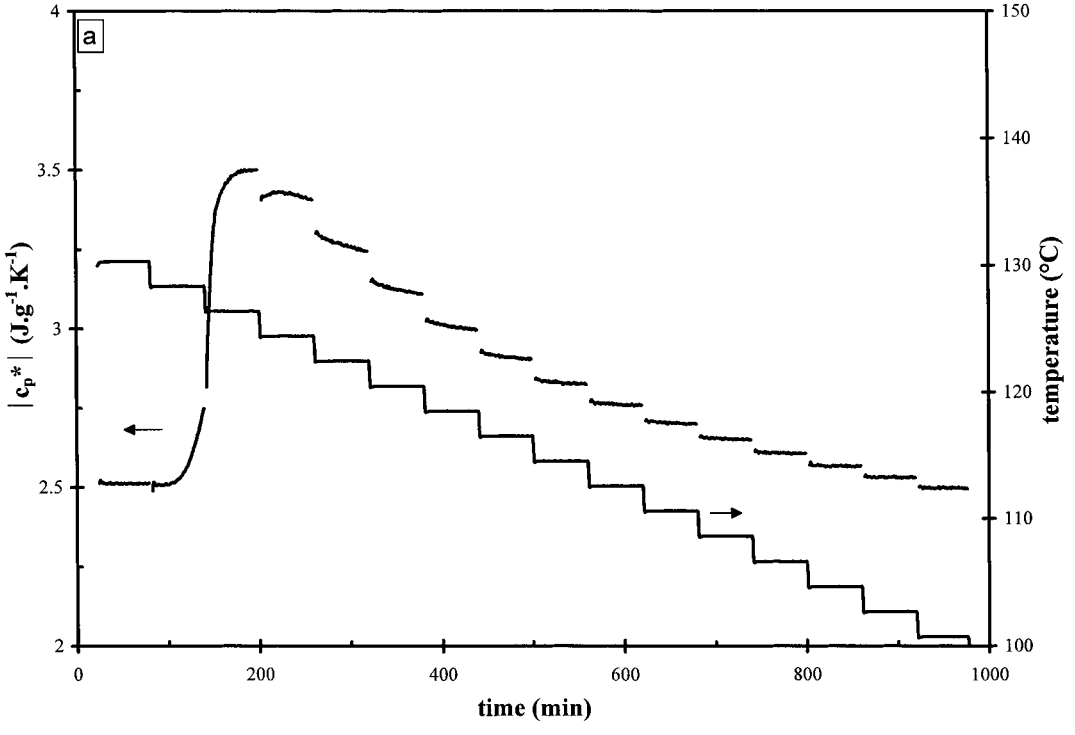

Fig. 10. Step-wise quasi-isothermal cooling (a) and heating (b) experiments of linear polyethylene (NIST SRM1484). Prior to the step-wise quasi-isothermal heating experiment (b), the sample was cooled down with 5°C/min. A repetitive temperature program was applied consisting of a temperature step of 2°C followed by a quasi-isothermal waiting time of 60 min. During the quasi-isothermal waiting time a sinusoidal temperature modulation was applied with A_T=0.4°C and p=60 s (TA Instruments).

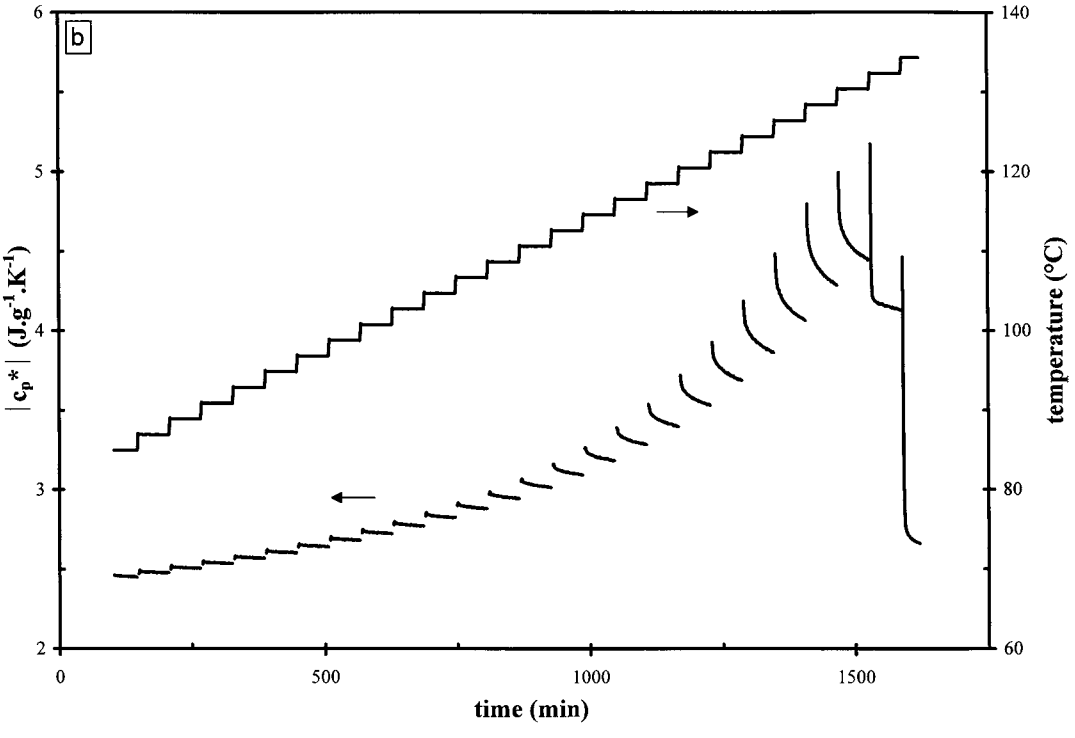

Fig. 10. (*Continued*)

significantly higher than the base-line capacity, implying that still a fraction of the crystalline material is susceptible to the temperature modulation even for such slow cooling rates. In analogy with the linear polyethylene (Fig. 10(b)), the reorganization during the quasi-isothermal waiting time proves to be appreciably smaller during cooling as compared with heating (Fig. 12(b)). The step-wise quasi-isothermal cooling experiment (Fig. 12(b)) also nicely manifests the crystallization at lower temperatures (80–100°C) of the fraction with a relatively higher comonomer content.

4. Conclusions

The experimental examples described in this paper nicely illustrate that the classification in three different regimes [41], simply based on the presence and temperature susceptibility of an excess process (i.e. $\partial w_i / \partial T_\omega$), proves to be very useful to identify and understand phenomena observed with TMDSC. These experiments also clearly demonstrate that TMDSC has added value in comparison with conventional DSC. However, this added value has to be put into the right perspective and differs between the regimes.

The determination of the absolute base-line capacity in regime I is, due to the intrinsic higher sensitivity of the technique, a potential advantage of TMDSC. Apart from the considerable larger measurement time involved with TMDSC, the accuracy proves to be in practice not significantly better as compared with conventional DSC [43]. Consequently, the only remaining advantage of TMDSC in regime I is its capability to study the frequency dependence of processes, although, the frequency range is often very limited in comparison with other dynamical techniques such as DMTA and DETA.

The ability to separate the base-line capacity from excess phenomena is undoubtedly a very valuable feature of TMDSC (regime II). Nonetheless, one has to realize that this feature is restricted to excess processes that are not susceptible to the temperature modulation such as for instance curing and enthalpy

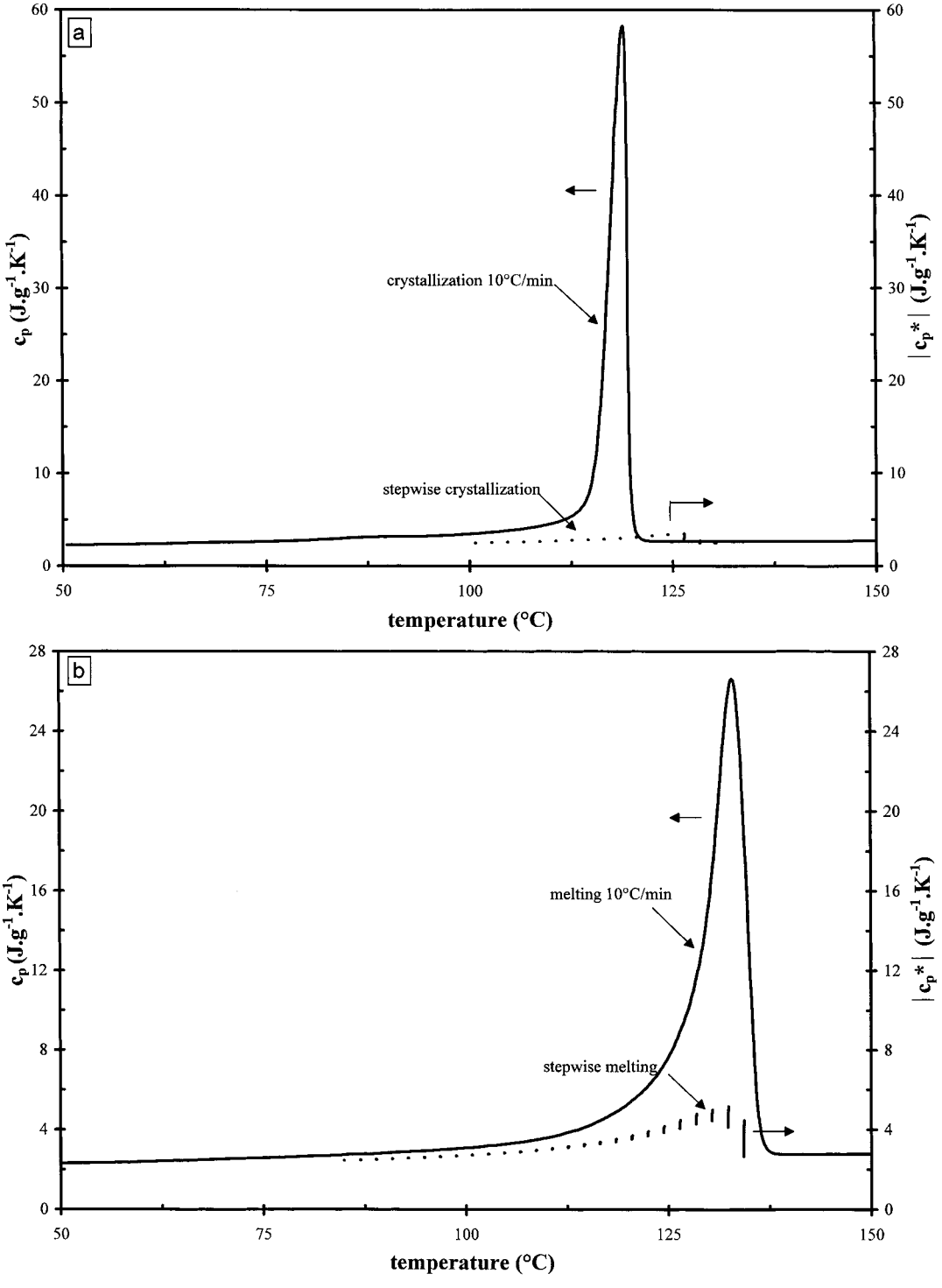

Fig. 11. Comparison of the heat capacity obtained with conventional DSC (10°C/min; Mettler) and $|c_p^*|$ acquired with step-wise quasi-isothermal TMDSC experiments during cooling (a) and heating (b) (cf. Fig. 10(a) and (b)).

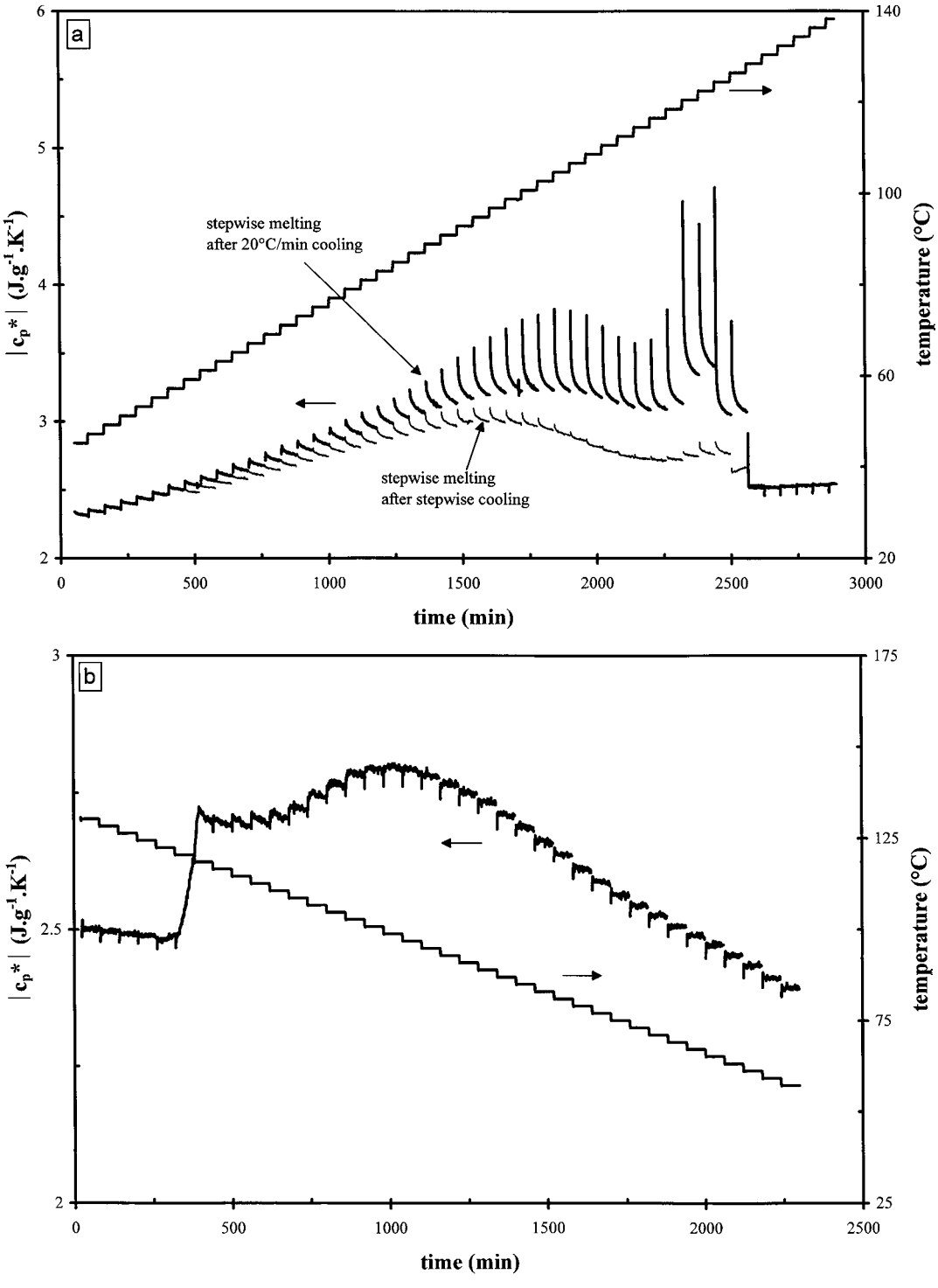

Fig. 12. Step-wise quasi-isothermal heating (a) and cooling (b) experiments of linear low density polyethylene (LLDPE). A repetitive temperature program was applied consisting of a temperature step of 2°C followed by a quasi-isothermal waiting time of 60 min. During the quasi-isothermal waiting time a sinusoidal temperature modulation was applied with A_T=0.4°C and p=60 s (TA Instruments).

recovery. Semi-crystalline polymers, on the other hand, exhibit an instantaneous excess heat flow response which can be ascribed to the reversible melting and crystallization of a few percent of crystalline material (regime III). This fraction proves to be dependent on the thermal history during heating. Although the base-line heat capacity can no longer be determined uniquely from $|c_p^*|$ in regime III, the latter provides in principle valuable information with respect to crystallization and melting. The question of linearity, the intrinsic violation of the required material invariance (i.e. $\partial w_i/\partial T_\omega \neq 0$) and the strong temperature dependence of the kinetics in combination with the generally large heat flow, imply that the conditions applied are very critical to obtain a reliable $|c_p^*|$. In that respect, the determination of an in- and out-of-phase heat capacity using the linear response is very critical in regime III. In spite of these serious limitations it has been demonstrated that TMDSC can provide additional insight in the crystallization and melting behaviour in case of (step-wise) quasi-isothermal measurements (i.e. $\beta_0=0$). Although this type of measurement is very time-consuming and can hardly be regarded as routine experiments, it contributes to a better understanding of the melting and crystallization mechanism. A more detailed study on the possible mechanism (e.g. surface melting [49,50]) connected with the observed reversible melting and crystallization phenomena will be presented in a subsequent paper [51].

5. Nomenclature

t	time
τ	characteristic time-scale of process
T	temperature
T_0	initial temperature; isothermal temperature
β	dT/dt=scanning rate
β_0	linear scanning rate
A_T	temperature amplitude
T_ω	modulated temperature variation ($A_T \sin \omega_0 t$)
T_β	linear temperature variation ($T_0+\beta_0 t$)
p	period
ω_0	$2\pi/p$
c_p	heat capacity
c_{p_b}	baseline heat capacity
c_{p_e}	excess heat capacity
w_i	mass fraction of phase i
h_i	enthalpy of phase i
$\partial w_i/\partial T_\omega$	variation of the mass fraction w_i due to the modulated temperature variation T_ω
$\partial w_i/\partial T_\beta$	variation of the mass fraction w_i due to the conventional temperature variation T_β
$\partial w_i/\partial t$	variation of the mass fraction w_i with time
Φ	total heat flow response
Φ_β	conventional heat flow response with linear scanning rate β_0
Φ_ω	modulated heat flow response
Φ_{isot}	conventional heat flow response at the isothermal temperature T_0
Φ_b	base-line heat flow response connected with base-line heat capacity
Φ_e	excess heat flow response connected with excess heat capacity
$\Phi_{b,\beta}$	conventional base-line heat flow response
$\Phi_{e,\beta}$	conventional excess heat flow response
$\Phi_{b,\omega}$	modulated base-line heat flow response
$\Phi_{e,\omega}$	modulated excess heat flow response
c_p'	in-phase heat capacity
c_p''	out-of-phase heat capacity
$\lvert c_p^* \rvert$	magnitude of the complex heat capacity
δ	phase angle
t_β	characteristic time-scale of linear underlying scanning rate β_0
t_ω	characteristic time-scale of temperature modulation

Acknowledgements

We gratefully acknowledge the financial support by the European Commission, grant 15CT96_0821.

References

[1] A. Boller, Y. Jin, B. Wunderlich, J. Thermal Anal. 42 (1994) 307.
[2] T. Ozawa, K. Kanari, Thermochim. Acta 288 (1996) 39.
[3] S.M. Marcus, R.L. Blaine, Thermochim. Acta 243 (1994) 231.
[4] S.R. Aubuchon, R.L. Blaine, Therm. Conduct. 23 (1996) 66.

[5] M. Song, A. Hammiche, H.M. Pollock, D.J. Hourston, M. Reading, Polymer 36 (1995) 3313.
[6] A. Boller, C. Schick, B. Wunderlich, Thermochim. Acta 266 (1995) 97.
[7] J.M. Hutchinson, S. Montserrat, J. Therm. Anal. 47 (1996) 103.
[8] A. Hensel, J. Dobbertin, J.E.K. Schawe, A. Boller, C. Schick, J. Therm. Anal. 46 (1996) 935.
[9] J.M. Hutchinson, S. Montserrat, Thermochim. Acta 286 (1996) 263.
[10] B. Wunderlich, A. Boller, I. Okazaki, S. Kreitmeier, J. Therm. Anal. 47 (1996) 1013.
[11] B. Wunderlich, I. Okazaki, Polym. Mater. Sci. Eng. 76 (1997) 217.
[12] D.J. Hourston, M. Song, A. Hammiche, H.M. Pollock, M. Reading, Polymer 37 (1996) 243.
[13] Y.P. Khanna, W.P. Kuhn, W.J. William, Macromolecules 28 (1995) 2644.
[14] S. Weyer, A. Hensel, J. Korus, E. Donth, C. Schick, Thermochim. Acta 304–305 (1997) 179.
[15] S. Weyer, A. Hensel, C. Schick, Thermochim. Acta 304–305 (1997) 267.
[16] S.L. Simon, G.B. McKenna, Thermochim. Acta 307 (1997) 1.
[17] G. van Assche, A. van Hemelrijck, H. Rahier, B. van Mele, Thermochim. Acta 286 (1996) 209.
[18] G. van Assche, A. van Hemelrijck, H. Rahier, B. van Mele, Thermochim. Acta 286 (1996) 209.
[19] M.-J. Shim, S.-W. Kim, Mater. Chem. Phys. 47 (1997) 198.
[20] G. Maistros, Q.P.V. Fontana, D. Attwood, J.S. Hudd, J. Mater. Sci. Lett. 16 (1997) 273.
[21] A. van Hemelrijck, B. van Mele, J. Therm. Anal. 49 (1997) 437.
[22] G. van Assche, A. van Hemelrijck, B. van Mele, J. Therm. Anal. 94 (1997) 57.
[23] G. van Assche, A. van Hemelrijck, H. Rahier, B. van Mele, Thermochim. Acta 304–305 (1997) 317.
[24] M. Song, A. Hammiche, H.M. Pollock, D.J. Hourston, M. Reading, Polymer 37 (1996) 5661.
[25] G.O.R. van Ekenstein, G. ten Brinke, T.S. Ellis, Polym. Mater. Sci. Eng. 76 (1997) 219.
[26] Y.Y. Cheng, M.V. Brillhart, P. Cebe, Thermochim. Acta 304–305 (1997) 369.
[27] M. Bonet, M. Buhk, G. Troegner, K.D. Rogausch, Acta Polym. 49 (1998) 174.
[28] S.R. Sauerbrunn, L. Thomas, Am. Lab. 27 (1995) 19.
[29] Y. Jin, J. Bonilaa, Y.-G. Lin, J. Morgan, L. McCracken, J. Carnahan, J. Therm. Anal. 46 (1996) 1047.
[30] I. Okazaki, B. Wunderlich, Macromol. Rapid Commun. 18 (1997) 313.
[31] I. Okazaki, B. Wunderlich, Macromolecules 30 (1997) 1758.
[32] A. Toda, T. Oda, S. Masamichi, Y. Saruyama, Polymer 38 (1997) 231.
[33] A. Toda, T. Oda, M. Hikosaka, Y. Saruyama, Thermochim. Acta 293 (1997) 47.
[34] J.E.K. Schawe, G.R. Strobl, Polymer 39 (1998) 3745.
[35] A. Wurm, M. Merzlyakov, C. Schick, Colloid Polym. Sci. 276 (1998) 289.
[36] J.E.K. Schawe, E. Bergmann, Thermochim. Acta 304–305 (1997) 179.
[37] B. Wunderlich, I. Okazaki, J. Therm. Anal. 49 (1997) 57.
[38] A. Toda, C. Tomita, M. Hikosaka, Y. Saruyama, Polymer 38 (1997) 2849.
[39] I. Okazaki, B. Wunderlich, Macromolecules 30 (1997) 1758.
[40] K. Ishikiriyama, B. Wunderlich, Macromolecules 30 (1997) 4126.
[41] R. Scherrenberg, V. Mathot, P. Steeman, J. Therm. Anal. 54 (1998) 477.
[42] National Institute of Standards and Technology, Standard Reference Material Program, SRM 1475/1484 – Linear Polyethylene, Gaitherburg, 1993.
[43] V.B.F. Mathot, M.F.J. Pijpers, J. Therm. Anal. 28 (1983) 349.
[44] V.B.F. Mathot, Polymer 25 (1984) 579; Errata Polymer 27 (1986) 969.
[45] B. Wunderlich, Pure Appl. Chem. 67 (1995) 1919.
[46] R.L. Scherrenberg, V.B.F. Mathot, A. van Hemelrijck, Lähnwitz seminar on temperature modulated DSC (1998).
[47] A. Wurm, M. Merzlyakov, C. Schick, Book of Abstracts ESTAC 7 (1998) 234.
[48] V.B.F. Mathot, Polycon 84 LLDPE, The Plastic and Rubber Institute, London (1984) 1.
[49] T. Albrecht, G.R. Strobl, Macromolecules 28 (1995) 5827.
[50] T. Albrecht, G.R. Strobl, Macromolecules 29 (1996) 783.
[51] R. Scherrenberg, B. Goderis, V. Mathot, A. van Hemelrijck, M. Koch, H. Reynaers, in preparation.